J. Fluid Mech. (1997), *vol.* 342, *pp.* 87–96. Printed in the United Kingdom

On an approximate model for the shape of a liquid–air interface receding in a capillary tube

By E. RAMÉ†
Department of Physics, Carnegie Mellon University, Pittsburgh, PA 15213, USA

(Received 2 February 1996 and in revised form 5 December 1996)

A good approximation to modelling the shape of a liquid–air meniscus advancing or receding in a capillary tube of radius a can be constructed by balancing the curvature of the interface with the sum of a viscous stress valid near the contact line and a constant static pressure. This model has unique solutions for each value of the boundary condition, i.e. the dynamic contact angle. When the meniscus recedes at very small capillary numbers, the model predicts a critical receding velocity beyond which a liquid layer of the receding fluid (a liquid tail) develops along the solid (see figure 4). The length of the layer increases as the receding speed and the contact angle decrease. This layer regime is characterized by menisci whose macroscopic curvature is $> 1/a$.

1. Introduction

It has been known for more than 20 years that the classical hydrodynamic assumptions give rise to a singular non-integrable stress tensor at the moving contact line formed by a fluid–fluid interface moving across a solid (Huh & Scriven 1971; Dussan V. & Davis 1974). This occurs whenever fluids modelled as incompressible and Newtonian are made to obey the no-slip condition at a rigid solid. The central consequence of this is the impossibility of satisfying a contact angle boundary condition at the moving contact line in the equation (discussed in §2) describing the shape of the fluid–fluid interface.

The singularity of the classical model implies that, in some small neighbourhood of the contact line (usually called the 'inner region'), new unique physics must arise. These new mechanisms are important in a characteristic length L_i surrounding the contact line. This need for new mechanisms which would generate a well-posed boundary value problem has prompted modifications of one or more of the classical hydrodynamic assumptions within a length scale L_i from the moving contact line (Dussan V., Ramé & Garoff 1991; Cox 1986). Unfortunately, identifying possible modification(s) is not a trivial matter because of the inability to experimentally probe the very small size L_i of the region where the classical assumptions fail.

In order to generate predictive calculations without knowledge of these unique new physical mechanisms, models postulate that, when the capillary number ($Ca \equiv U\mu/\sigma$, where U is the speed of the solid relative to the contact line, μ is the viscosity and σ is the surface tension) is small, there exists a region very near the contact line where the fluid–fluid interface deformation by viscous forces is independent of the system geometry and usual hydrodynamics controls the fluid motion (Cox 1986; Pismen & Nir 1982; Hocking & Rivers 1982). This region, called the 'intermediate region', lies very near the moving contact line but not so close that the classical model fails. This notion rests on the assumption that, regardless of the macroscopic geometry,

† Present Address: NASA Lewis Research Center, MS 500-102, Cleveland, OH 44135, USA.

all flows have the same structure in the limit as the contact line is approached. This limiting flow structure is only determined by the wedge-like geometry defined between the solid wall and the fluid–fluid interface.

The presence of the intermediate region arises in the limit $Ca \to 0$, with $Ca \ln(a/L_i) = O(1)$, where L_i is the length scale of the inner region and a is the scale of the macroscopic, or 'outer', region, a role played here by the tube radius. In this limit, most of the macroscopic interface looks static, with viscous deformation being important only in the geometry-free intermediate region near the contact line (Dussan V. *et al.* 1991; Marsh, Garoff & Dussan V. 1993; Chen, Ramé & Garoff 1995). The interface shape in the intermediate region where viscous forces are large and independent of geometry depends solely on the material system (which may introduce additional dynamics besides the purely hydrodynamic dependence described by Ca) and on Ca. Thus, the interface shape in this region constitutes a dynamic material property which may be used to form a boundary condition for the macroscopic interface shape in any geometry. In this way, the interface slope at any point in this geometry-independent region can be used as a dynamic contact angle in a well-posed boundary value problem.

Dussan V. *et al.* (1991) developed a model for the interface shape near the contact line formed by a soid entering a large liquid bath. This model is only valid near the moving contact line where geometry-free viscous and static-like contributions both play a role. Although the model does not apply in the outer or macroscopic region, it might be appealing to use it to construct the whole interface shape formed in the gap between two parallel plates or in a capillary tube. This path was pursued by Boender, Chesters & van der Zanden (1991) for liquid displacing air (advancing motions) and by Chesters & van der Zanden (1993, referred to herein as CZ) for air displacing liquid (receding motions).

In this paper we examine the receding fluid mode in detail using an approach similar but not identical to that of CZ. We discuss the difference in physical situations arising when fluid advances or recedes against a gas of negligible viscosity. The model examined here shows that, when $Ca \ll 1$, receding motions are qualitatively different from and have a dynamic behaviour much richer than advancing motions. Our model, presented in §2, shows the development of a liquid layer left behind when the liquid recedes above a critical speed as illustrated in figure 4. In §3 we discuss the characteristics of the liquid layer, and state our conclusions in §4.

2. Formulation and solution

A simplified expression describing a dynamic meniscus in a capillary tube of radius a in the limit of zero gravity (or vanishingly small Bond number $Bd \equiv \rho g a^2/\sigma$, where ρ is the density, g the acceleration due to gravity and a the tube radius) is the following *ad hoc* version of the normal component of the dynamic boundary condition (i.e. the balance of surface tension by the normal stresses exerted by the fluid on the fluid–air interface):

$$\frac{1}{1-x}\frac{\mathrm{d}[(1-x)\cos(\theta)]}{\mathrm{d}(1-x)} = Ca\frac{2\sin^2(\theta)}{\theta-\sin(\theta)\cos(\theta)}\frac{1}{x}+B, \tag{1a}$$

subject to boundary conditions

$$\theta = \pi/2 \quad \text{at} \quad x = 1, \tag{1b}$$

$$\theta = \theta^* \quad \text{at} \quad x = x^*, \tag{1c}$$

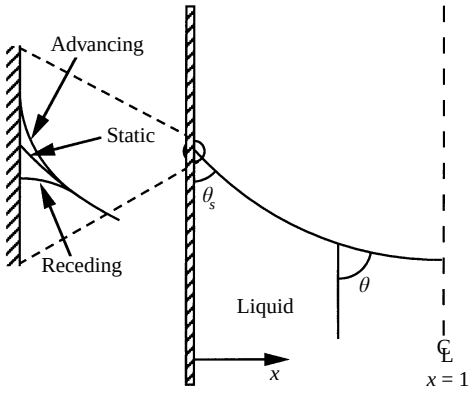

FIGURE 1. Coordinate system used in this study and qualitative sketch of static, advancing and receding shapes. The region of viscous deformation is greatly magnified. The two dynamic contact angles are such that the macroscopic dynamic shapes coincide with a static shape with contact angle θ_s.

where $x \equiv 1-r$, with r the radial coordinate measured perpendicularly away from the centreline, made dimensionless with the tube radius; θ is the angle between the tangent to the meniscus and the tube wall measured through the liquid, and B is a constant whose value is part of the solution to (1 *a–c*) (see figure 1).

The different terms of (1 *a*) are as follows. The left-hand side is the curvature of an axisymmetric meniscus in a capillary tube. The first term on the right-hand side is the viscous contribution to the normal stress. It arises in the context of a formal asymptotic expansion valid in the intermediate region, where viscous and surface tension forces balance to lowest order as $Ca \to 0$ (Hocking & Rivers 1982; Pismen & Nir 1982; Cox 1986). The constant B equals the static curvature in the absence of viscous effects and corresponds to the static part of the normal stress on the interface. This contribution should be important near the tube centre when $Ca \ll 1$.

Boundary condition (1 *b*) states that the slope of the meniscus is continuous at the centreline; whereas (1 *c*) plays the role of a contact angle, θ^*, applied at a non-zero distance from the wall, x^*. Because of the singularity discussed above, the contact angle cannot be imposed at the moving contact line ($x = 0$). Following CZ, we adopt $x^* \sim \mathrm{e}^{-15}$, which is consistent with a tube radius of a few millimetres and a cut off of a few Angstroms next to the solid.†

At $Ca \neq 0$, equation (1) is strictly valid only very near the contact line, where $x \ll 1$ and the viscous normal stresses are given by the flow in a wedge (Moffatt 1964; Cox 1986). Nevertheless, (1) is a good approximation for $0 < x < 1$ in the limit $Ca \to 0$ as the $1/x$ decay of the viscous term confines its importance to the close vicinity of the contact line, with a small error introduced near the tube centre.

One way of solving (1) is to eliminate B by differentiating with respect to $(1-x)$. The only caveat is that, since the interface shape θ is itself a function of x, one needs to apply the chain rule when differentiating the θ-dependent coefficient of Ca in (1 *a*). Another way – which we have adopted here – would be not to eliminate B and to solve

† While in principle a contact angle can be imposed at any point on the interface, not all parts of the interface shape are suitable for imposing a contact angle *material property*. A *material* dynamic contact angle must be applied very near the moving contact line where the interface is geometry independent. Thus, in order for θ^* to act as a material boundary condition in (1), its location x^* must lie in the region where the viscous interfacial deformation is much larger than the static contribution, B. Many theoretical investigators have chosen x^* to be of molecular dimensions (CZ).

the problem as given in (1 *a–c*). In our calculations, we fix B and integrate (1 *a*) directly as an initial value problem subject to $\theta = \pi/2$ at $x = 1$, using a fourth-order Runge–Kutta formula. (All of our calculations are accurate to at least five decimal figures.) For each B, we then get θ^* from the solution as the slope at $x = x^*$. Thus, the macroscopically observable shape described by B is set by the contact angle θ^* (a dynamical material property, possibly dependent on U) and by Ca.

3. Results and discussion

Figure 2 shows the relation between contact angle θ^* and the centreline meridian curvature, $\eta_c (\equiv \mathrm{d}\theta/\mathrm{d}x$ at $x = 1)$ for a static meniscus and for several advancing ($Ca > 0$) and receding ($Ca < 0$) motions. In a capillary tube, η_c and B are related by: $\eta_c = \frac{1}{2}(B + Ca\,4/\pi)$. When the meniscus is static, i.e. $Ca = 0$, the meniscus is circular and the contact angle is related to the curvature by $\theta^* = \cos^{-1}(\eta_c)$. When the meniscus is in motion, viscous deformation near the contact line alters this relationship. In figure 2, the lines of θ^* *vs.* η_c in advance approach the static curve ($Ca = 0$) uniformly as $Ca \to 0^+$, while the lines in recession do so only over a certain range of θ^* as $Ca \to 0^-$. (The + and − superscripts denote the approach to zero from above and below, respectively.) This marks a fundamental difference between advancing and receding motions in the model of equation (1).

To understand this difference we must discuss the viscous deformations for each motion. This difference comes from the fact that the curvatures from viscous forces in advancing and receding motions have opposite signs. We begin with the advancing case because it has the simpler regime for the Ca values studied.

When the meniscus advances ($Ca > 0$), viscous forces very near the contact line open the angle between the fluid–fluid interface and the wall above the angle that would exist in a purely static interface with the same contact angle θ^*. Far from the contact line, as viscous forces become negligible, the interface shape enters the macroscopic static-like region. At this point, the advancing interface has a larger slope θ than a wholly static interface with the same contact angle θ^*. Figure 3 illustrates this with one static and several advancing shapes, all having a 30° contact angle. The central consequence of the viscous deformation in advance is that the centreline curvature of the meniscus is always smaller than that of a static interface with the same contact angle (figure 3), implying that in advance η_c is always < 1 for any $\theta^* \geqslant 0$.

All advancing shapes (but not all receding shapes, as we discuss below) have the feature that the viscous deformation is confined to a microscopic region near the contact line. To the eye one perceives an *apparent* contact angle, $\theta_{app} \equiv \cos^{-1}(\eta_c) > 0$, where η_c is the curvature of the macroscopic static-like meniscus (see dashed lines in figure 3). Thus, the static-like macroscopic advancing meniscus appears to intersect the tube wall at a well-defined (albeit not the actual) contact line (figure 1). Even though the viscous deformation is microscopic, it can be so drastic as to change the sign of the interface curvature. For example, for any fixed $\theta^* < 90°$, there exists a Ca beyond which the centreline curvature is negative, i.e. the naked eye perceives an apparent contact angle $> 90°$ (figure 2 and line with $Ca = 0.07$ in figure 3). It is precisely because the macroscopic menisci have a well-defined apparent contact angle which approaches the static value as $Ca \to 0^+$ that the θ^* *vs.* η_c lines in figure 2 approach the static line uniformly in advance as $Ca \to 0^+$.

Receding motions are more complex than advancing ones at low Ca. When the meniscus recedes ($Ca < 0$), the direction of viscous deformation near the moving contact line is opposite to that in the advancing case. Thus, viscous deformation in

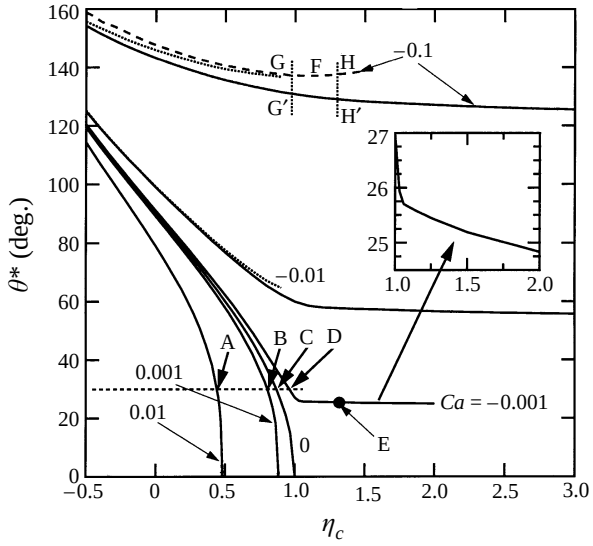

FIGURE 2. Interface slope, θ^*, near the contact line at $x^* = e^{-15}$, *vs.* centreline meridian curvature for various Ca in advancing and in receding modes: ——, this work; – – –, CZ; ·····, asymptotic analysis, $Ca = -0.1$. The asymptotic analysis is indistinguishable from the model for the other Ca values shown. Point E corresponds to figure 4(*a*) and to curve 2 in figure 5.

recession closes the angle, θ, between the dynamic interface and the solid relative to a wholly static interface with the same contact angle θ^*. As a consequence, the slope θ of a receding meniscus as it enters the static-like region far from the contact line is smaller than that of a static interface with the same contact angle (figure 3).

This opposite direction of the viscous effects makes receding motions dynamically richer than advancing ones. Figure 2 shows that the lines of θ^* *vs.* η_c in recession hug the static line $Ca = 0$ as $Ca \to 0^-$ only when θ^* is more that some critical value θ^*_{crit} (figure 2). θ^*_{crit} corresponds to $\eta_c \sim 1$, i.e. a 0° apparent contact angle.

Thus, receding menisci have two regimes depending on whether $\theta^* > \theta^*_{crit}$ or $\theta^* < \theta^*_{crit}$. The first regime, characterized by $\theta^* > \theta^*_{crit}$ ($\eta_c \leqslant 1$), is not a special case. In fact, it is analogous to the advancing case in that the viscous deformation is confined to a microscopic region near the contact line, and the naked eye perceives the macroscopic part of the meniscus as intersecting the tube wall with a well-defined contact angle θ_{app} (see e.g. point D in figure 2 and line D in figure 3). The second regime, characterized by $\theta^* < \theta^*_{crit}$ ($\eta_c > 1$), is unique to receding motions. Contrary to $\eta_c < 1$, here a static meniscus with curvature $\eta_c > 1$ cannot intersect the tube wall because $\eta_c > 1$ corresponds to a circular meniscus with radius < 1, i.e. smaller than the tube radius. Since this leaves a 'gap' between the static-like region and the wall, no well-defined θ_{app} can exist.

Our model shows that receding menisci with $\theta^* < \theta^*_{crit}$ are special in that they can sustain centreline curvatures $\eta_c > 1$. This ability is entirely due to the direction of viscous deformation in recession which bridges the 'gap' between the wall and the static shape with $\eta_c > 1$. The nature of the interface deformation in recession with $\theta^* < \theta^*_{crit}$ ($\eta_c > 1$) is fundamentally different from that of the deformation in advancing menisci and in receding menisci with $\theta^* > \theta^*_{crit}$ because, in order to bridge this gap, viscous effects must necessarily extend into the macroscopic scale. The 'bridge' between the quasi-static meniscus and the tube wall appears in the form of a thin, usually long, liquid layer nearly parallel to the tube wall, and is characterized by angles $\theta \sim 0$ (figure 4).

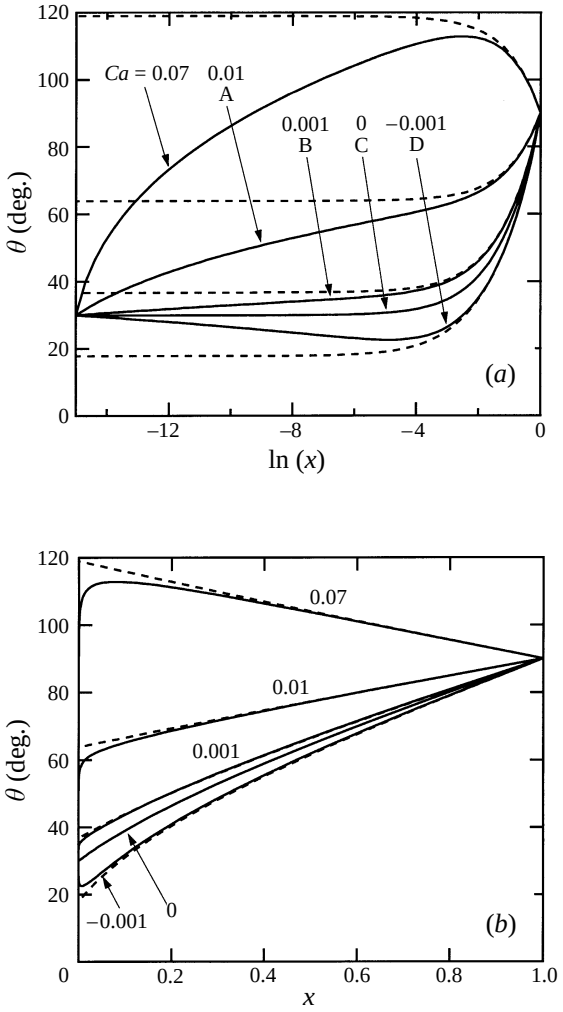

FIGURE 3. ——, Advancing ($Ca > 0$), static ($Ca = 0$) and receding ($Ca < 0$) menisci with contact angle $\theta^* = 30°$. – – –, Static shapes having the same centreline curvature as the corresponding dynamic shapes. (*a*) Semi-log scale shows viscous region in detail; (*b*) linear scale shows macroscopic region in detail. The numbers denote *Ca*. The letters A–D correspond to the points with the same letter in figure 2.

For each $Ca < 0$, the layer length increases with $\theta^*_{crit} - \theta^*$. Figure 5 shows the dynamic shapes for $Ca = -0.001$ at contact angles, θ^*, such that $\eta_c = \{0.98, 1.1, 1.3\}$, together with the static shapes corresponding to each η_c. When $\theta^* = 27°$ ($\eta_c = 0.98$) the viscous deformation is confined to a very small region near the wall and a liquid tail does not form. As discussed above, this occurs with all advancing motions and with those receding motions for which $\eta_c \leqslant 1$. In contrast, when $\theta^* = 25.64°$ ($\eta_c = 1.1$), a layer with length ~ 2 develops, whereas when $\theta^* = 25.4°$ ($\eta_c = 1.3$) the layer length is ~ 13 (figure 4). The sensitivity of the layer length to the contact angle θ^* is very high and increases as $Ca \to 0^-$.

When a layer develops, viscous effects penetrate well into the tube. For example, when $\eta_c = 1.3$ (point E in figure 2 and curve 2 in figure 5), the liquid tail extends into at least 23 % of the tube radius owing to the viscous term in (1*a*). A static-like meniscus arises for $0.23 \lesssim x < 1$. At $x \sim 0.23\,(= 1 - 1/\eta_c)$, the static-like meniscus ceases to

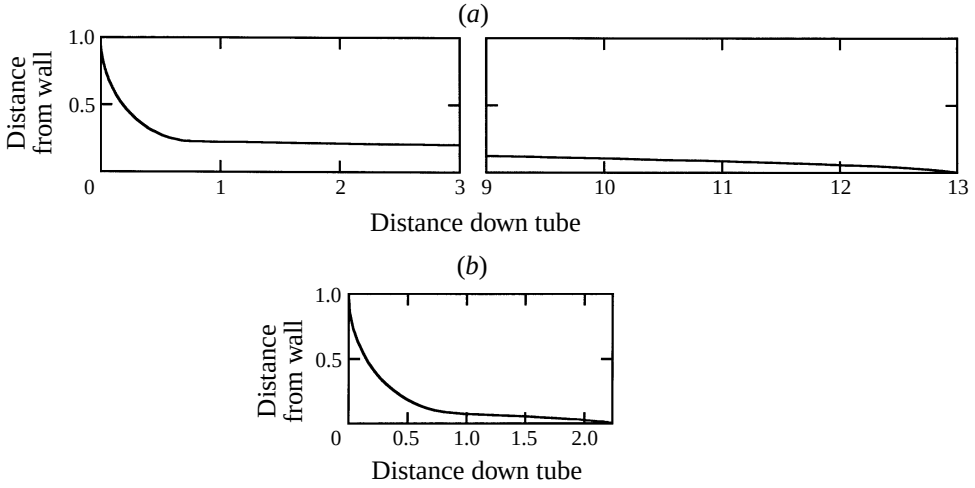

FIGURE 4. Dynamic meniscus at $Ca = -0.001$: (*a*) $\theta^* = 25.4°$ (causing $\eta_c = 1.3$); (*b*) $\theta^* = 25.64°$ (causing $\eta_c = 1.1$).

exist; and for $x \lesssim 0.23$ (i.e. between the end of the quasi-static shape and the wall), the liquid tail develops nearly parallel to the wall. This layer corresponds to the portion of line 2 in figure 5 where $\theta \sim 0$. The transition at $x \sim 0.23$ is smooth despite its sharp appearance in figure 5. In the range of x where the quasi-static meniscus exists, θ increases very quickly and viscous effects are virtually zero.

Although viscous effects appear at x as large as 0.23, viscous forces deform the interface significantly only for $x < 0.05$, where the viscous term balances the curvature in (1*a*) to meet the required value of θ^*. Most of the action of viscous forces in $0.05 < x < 0.23$ is to develop a liquid layer nearly parallel to the wall. In this nearly parallel portion, the terms on the right-hand side of (1*a*) add up to almost zero so that the shape behaves as $\theta \sim (-3Caz/B)^{1/2}$ for $\theta \ll 1$ and $z \gg 1$, where z is the axial distance from the contact line. Only when the layer thickness is small enough, i.e. after a long tail has developed, does the final deformation meeting the desired θ^* take place. The presence of this 'similarity' region explains the increasingly high sensitivity of the layer length to the contact angles as $Ca \to 0^-$.

The picture that emerges from figure 5 is that, when $\theta^* < \theta^*_{crit}$, essentially the same basic liquid layer shape (with minuscule variations in θ^* but significantly different lengths) gives rise to all macroscopic menisci with $\eta_c > 1$. In order to meet the quasi-static meniscus, the layer adjusts its own length in response to very small variations in θ^*. Thus, based on this model, the layer must be longer the closer Ca is to zero (for fixed $\eta_c > 1$), or the smaller the value of θ^* (for fixed Ca) (refer to figure 4).

Solutions of (1) for receding menisci ($Ca < 0$) have the peculiarity that, for $\theta^* < \theta^*_{crit}$, the curves η_c *vs.* θ^* do not uniformly approach the static case, $Ca = 0$. In fact, for $Ca \to 0^-$: (i) the transition in the curves η_c *vs.* θ^* gets progressively sharper; and (ii) the thin liquid layer gets progressively longer for fixed $\theta^* - \theta^*_{crit} < 0$. This strongly suggests that the limit $Ca \to 0^-$ of (1) is singular, with a 'boundary layer' thickness that gets smaller as $Ca \to 0^-$. However, the 'long-z' scaling derived from (1*a*), $\theta \sim Ca^{1/2}$, is incompatible with the standard lubrication scaling, $\theta \sim Ca^{1/3}$, which raises questions as to the proper asymptotic treatment of this model.

In all cases we found that for each θ in recession there exists only one value of η_c consistent with a steady-state solution. This contrasts with CZ's results (dashed line in

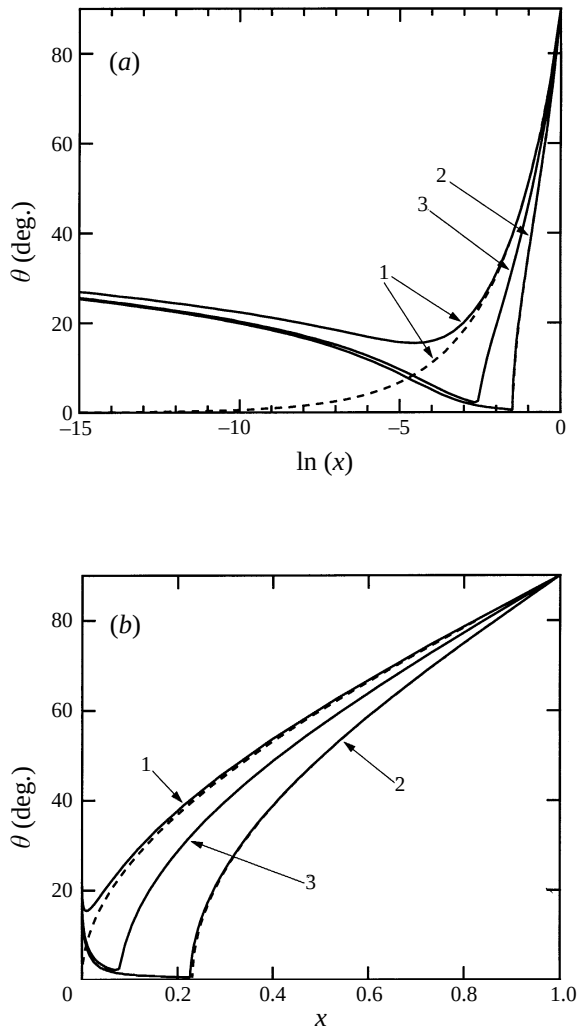

FIGURE 5. Interface shapes, θ, *vs.* distance from the wall: (*a*) semi-log scale shows viscous region in detail; (*b*) linear scale shows macroscopic region in detail. Shapes are for three values of the contact angle θ^* causing different η_c: curve 1, $\eta_c = 0.98$; 2, $\eta_c = 1.3$; 3, $\eta_c = 1.1$. ——, Dynamic ($Ca = -0.001$); – – –, static, same η_c as dynamic. At $\eta_c = 1.3$, the static shape is indistinguishable from the quasi-static part of the dynamic shape.

figure 2), who found that: (*a*) below a certain θ^* (point F, figure 2) no solution exists, and (*b*) two receding menisci can have different shapes (i.e. different η_c) with the same contact angle θ^* (compare points G, H with our results G′, H′). In order to eliminate B from the problem, CZ differentiated (1) with respect to x, neglecting a term that arises because $\theta = \Theta(x)$. This term is always negligible except when $Ca < 0$ and $\theta^* < \theta^*_{crit}$ ($\eta_c > 1$), which invalidates CZ's results for $\eta_c > 1$. Thus, it remains to be determined whether, in recession and with $\theta^* < \theta^*_{crit}$, there exists another critical value of θ^* below which: (*a*) no steady solution can exist, or (*b*) a steady solution exists but is unstable. The cut-off Ca for the existence of solutions to the model equation appears to be the value of $Ca < 0$ at which the curvature at the centre of the tube is infinite. Our calculations never reach this point, where the model (1) may well be invalid. This cut-off is different from the one implied in asymptotic models, given in

figure 2 roughly by the kink of the $Ca < 0$ lines (Cox 1986). To lowest order, the asymptotic matching process generates a boundary condition for the static-like macroscopic meniscus in the form of an apparent contact angle. This apparent contact angle is necessarily $\geqslant 0$ (Dussan V. *et al.* 1991; Cox 1986), hence a centreline curvature $\eta_c > 1$ is meaningless in the context of matched asymptotics. To the right of the kink, however, solutions to the model equation continue to exist but the character of the meniscus changes through this kink.

Equation (1) is the *ad hoc* extension of the standard matched asymptotic approach for a capillary tube geometry. Thus, we expect calculations based on (1) to be a good approximation when $|Ca| \ll 1$ as long as $\eta_c \leqslant 1$, i.e. for advancing menisci at any θ^*, and for receding menisci at $\theta^* > \theta^*_{crit}$ (figure 2). Equation (1) should also work for θ^* just below θ^*_{crit}, when the layer near the wall has not yet developed. In fact, (1) agrees well with Lowndes' (1980) finite element calculations of advancing menisci and with approximate solutions obtained using matched asymptotic expansions for $0 < Ca \leqslant 0.07$ (Dussan V., personal communication).

4. Conclusions

We have presented an approximate model describing the shapes of advancing and receding liquid–air menisci in a capillary tube. The model is strictly valid as $Ca \to 0$, very near the moving contact line where the term proportional to Ca in (1*a*) describes viscous deformation (Chen *et al.* 1995). The approximation of the model consists of using the same model throughout the tube.

In the limit $|Ca| \to 0$, the model agrees with experimentally verified asymptotic analyses for any θ^* in advance and for $\theta^* > \theta^*_{crit}$ (i.e. $\eta_c \lesssim 1$) in recession (figure 2) (Dussan V. *et al.* 1991; Marsh *et al.* 1993; Chen *et al.* 1995). Under these conditions, the term proportional to Ca in (1*a*) is important only where x is small, and the model is consistent with asymptotic analyses. However, when a long tail of liquid is left behind in recession, this term appears to play a role even when x is not small, but the usual asymptotic analyses cannot address this regime. This opens the possibility that, under conditions such that a tail forms, additional terms of $O(Ca)$, which do not arise in current asymptotic treatments, might be important.

What is, then, the physical relevance of those combinations $\{\theta^*, Ca\}$ producing $\eta_c > 1$? One should recall that (1) is strictly incorrect. However, it can be a good approximation when $|Ca| \ll 1$ provided: (*a*) the viscous effects it predicts are confined to a very small region near the contact line where the coefficient of Ca in (1*a*) is valid; or (*b*) in the liquid layer $Ca \ll \theta^2$, a condition for the validity of the viscous term in (1*a*) met by all of our calculations including those where a tail develops. For each fixed $Ca < 0$ and $\theta^* < \theta^*_{crit}$, the model has a unique solution and predicts the qualitatively correct development of a liquid layer next to the solid. The length of the tail increases as $Ca \to 0^-$ or as θ^* decreases. The model also predicts Ca_{crit}, such that the liquid layer of the receding fluid develops next to the wall for fixed θ^* and $Ca < Ca_{crit} < 0$.

The layer calculated in this study is not the same as the layer of 'infinite length' and uniform thickness studied by Bretherton (1961). This layer with uniform thickness does not have an explicit end. If we were to conceive its end, it might have a region of decreasing thickness and a contact line pinned to the solid. This should make the whole liquid layer move as a rigid body at the solid velocity. Considered globally, this flow is unsteady because the layer length increases in time. Another possible end for the infinite layer is a region near the contact line where fluid accumulates near a contact line fixed in space. This situation is also unsteady because a ridge thicker than the

Bretherton layer must propagate from the contact line down to the bulk fluid. Our calculations, on the other hand, are steady solutions. Contrary to the scenarios described above, the net flow across any section of the layer is zero in this study, hence both the layer length and shape are constant in time. It remains to determine the relation (or lack thereof) between the lubrication layer produced in our calculations and the class of lubrication layers of Bretherton.

I would like to acknowledge S. Garoff, E. B. Dussan V. and A. Bose for their always insightful comments. I would also like to acknowledge NASA's financial support under grant No. NAG3-1390.

REFERENCES

Boender, W., Chesters, A. K. & Zanden, A. J. J. van der 1991 An approximate analytical solution of the hydrodynamic problem associated with an advancing liquid-gas contact line. *Intl J. Multiphase Flow* **17**, 661–676.

Bretherton, F. P. 1961 The motion of long bubbles in tubes. *J. Fluid Mech.* **10**, 166–188.

Chen, Q., Ramé, E. & Garoff, S. 1995 The breakdown of asymptotic models of liquid spreading at increasing capillary number. *Phys. Fluids* **7**, 2631–2639.

Chesters, A. K. & Zanden, A. J. J. van der 1993 An approximate analytical solution of the hydrodynamic problem associated with receding liquid-gas contact lines. *Intl J. Multiphase Flow* **19**, 905–912 (referred to herein as CZ).

Cox, R. G. 1986 The dynamics of the spreading of liquids on a solid surface. Part 1. Viscous flow. *J. Fluid Mech.* **168**, 169–194.

Dussan V., E. B. & Davis, S. H. 1974 On the motion of a fluid–fluid interface along a solid surface. *J. Fluid Mech.* **65**, 71–95.

Dussan V., E. B., Ramé, E. & Garoff, S. 1991 On identifying the appropriate boundary conditions at a moving contact line: an experimental investigation. *J. Fluid Mech.* **230**, 97–116.

Hocking, L. M. & Rivers, A. D. 1982 The spreading of a drop by capillary action. *J. Fluid Mech.* **121**, 425–442.

Huh, C. & Scriven, L. E. 1971 Hydrodynamic model of steady movement of a solid/liquid/fluid contact line. *J. Colloid Interface Sci.* **35**, 85–101.

Lowndes, J. 1980 The numerical simulation of the steady movement of a fluid meniscus in a capillary tube. *J. Fluid Mech.* **101**, 631–646.

Marsh, J. A., Garoff, S. & Dussan V., E. B. 1993 Dynamic contact angles and hydrodynamics near a moving contact line. *Phys. Rev. Lett.* **70**, 2778–2781.

Moffatt, H. K. 1964 Viscous and resistive eddies near a sharp corner. *J. Fluid Mech.* **18**, 1–18.

Pismen, L. M. & Nir, A. 1982 Motion of a contact line. *Phys. Fluids* **25**, 3–7.

Ramé, E. & Garoff, S. 1995 Microscopic and macroscopic dynamic interface shapes and the interpretation of dynamic contact angles. *J. Colloid Interface Sci.* **177**, 234–244.